

# Nanoscale

Accepted Manuscript



This is an *Accepted Manuscript*, which has been through the Royal Society of Chemistry peer review process and has been accepted for publication.

*Accepted Manuscripts* are published online shortly after acceptance, before technical editing, formatting and proof reading. Using this free service, authors can make their results available to the community, in citable form, before we publish the edited article. We will replace this *Accepted Manuscript* with the edited and formatted *Advance Article* as soon as it is available.

You can find more information about *Accepted Manuscripts* in the [Information for Authors](#).

Please note that technical editing may introduce minor changes to the text and/or graphics, which may alter content. The journal's standard [Terms & Conditions](#) and the [Ethical guidelines](#) still apply. In no event shall the Royal Society of Chemistry be held responsible for any errors or omissions in this *Accepted Manuscript* or any consequences arising from the use of any information it contains.

Assessing the improved performance of  
freestanding, flexible graphene and carbon nanotube  
hybrid foams for lithium ion battery anodes

Adam P. Cohn<sup>1</sup>, Landon Oakes<sup>1,2</sup>, Rachel Carter<sup>1</sup>, Shahana Chatterjee<sup>1</sup>, Andrew Westover<sup>1,2</sup>,  
Keith Share<sup>1,2</sup>, and Cary L. Pint<sup>1,2,\*</sup>

<sup>1</sup> *Department of Mechanical Engineering, Vanderbilt University, Nashville, TN 37235*

<sup>2</sup> *Interdisciplinary Materials Science Program, Vanderbilt University, Nashville, TN 37235*

*\*Corresponding author: cary.l.pint@vanderbilt.edu*

**Abstract**

We demonstrate the fabrication of three-dimensional freestanding foams of hybrid graphene-single-walled carbon nanotube nanomanufactured materials with reversible capacities of 2640 mAh/g at 0.186 A/g and 236 mAh/g at 27.9 A/g. The Li storage behavior of this material is compared against other nanostructures in similar flexible foam platforms including graphene, ultra-thin graphite, and single-walled carbon nanotubes (SWNTs), and we elucidate the improved hybrid material performance due to the decoupling of lithium storage reaction energetics dictated by the SWNTs from the total storage capacity of the hybrid material. This work demonstrates a route to develop mechanically robust all-carbon electrodes with the potential for reversible Li-ion storage capacity approaching silicon, power capability of the best supercapacitors, and based on a material simultaneously usable as a charge collector and anode.

## I. Introduction

The prospect for next-generation lithium-ion batteries that can store substantially greater amounts of energy than current Li-ion technology and charge in a matter of seconds, rather than hours, is dictated by innovation in the electrode materials implemented into devices.<sup>1-4</sup> Current lithium-ion battery technology utilizes thin, micron-scale coatings of graphite as anode materials enabling a maximum reversible capacity of 372 mAh/g. The prospect for improving this performance with alternative materials has spurred a massive research thrust in recent years, with Si materials receiving the most attention for their ultra-high bulk 4200 mAh/g maximum capacity and ~ 3600 mAh/g capacity achievable at room temperature.<sup>5, 6</sup> However, silicon materials can often be limited to short cycle lifetimes attributed to solid electrolyte interphase layer (SEI) growth that compromises performance and cyclability. In this regard, carbon nanomaterials such as graphene or carbon nanotubes possess an inherent electrochemical stability that yields favorable SEI layer formation,<sup>1, 3, 7, 8</sup> even though the optimal capacity for storage in these materials remains unknown. Numerous previous reports exist highlighting the promise for graphene and single-walled carbon nanotubes as anodes in reversible Li-ion batteries.<sup>7, 9-20</sup> Most reports emphasize reversible capacities between 500-1200 mAh/g, with reports of capacities reaching up to 1723 mAh/g.<sup>10</sup> Graphene-based materials have also been demonstrated to display exemplary rate capabilities of up to 235 mAh/g at rates of 25 A/g.<sup>15</sup>

Whereas these results give extraordinary promise to nanostructured carbons as advanced energy carriers, the origin of the high capacities obtained in these materials is not well understood. Recent work emphasizes the role defects play in graphene to enable improved capacities,<sup>10</sup> which is independently supported by studies where doping of the lattice has been achieved with both N- or B- atoms to yield improve storage behavior.<sup>15</sup> Another possibility is

the importance of the few-layered graphene interlayer spacing that can enable such capacities, which may be modified in hybrid structures.<sup>16</sup> Recent density functional theory calculations have emphasized the capability of Li to cluster<sup>21, 22</sup> and diffuse rapidly across edges that appear in thin graphene materials giving promise to high power storage.<sup>23</sup> Nonetheless, there is no current understanding of what physical mechanisms limit or aid in the storage capacity of nanostructured carbons, leaving no identifiable capacity goal for these materials as viable energy carriers. Furthermore, unlike bulk intercalation storage materials where the surface or solid electrolyte interphase (SEI) region dictates chemical reaction pathways while the bulk material properties dictate the total storage capacity, all characteristics for lithium storage in carbon nanomaterials are dictated by surface properties – emphasizing the importance of controlling these properties to make realizable electrode materials.

In this study, we develop pristine, defect-free hybrid graphene-SWNT freestanding materials and find them to exhibit capacities approaching that of the best bulk materials (2640 mAh/g @ 0.186 A/g) with simultaneous excellent rate capability (236 mAh/g @ 27.6 A/g). To assess the mechanism behind this excellent storage capability, we characterize these results in the framework of three other identically prepared carbon materials: graphene foams, SWNT foams, and ultra-thin graphite foams. We observe that the hybrid materials support greater lithium storage capability due to a combination of the greater reactivity of the SWNTs combined with the increased capacity of the graphene-SWNT combined hybrid material.

## II. Experimental Methods

### Materials Fabrication

To grow few-layered graphene and ultra-thick graphene materials on nickel foams, chemical vapor deposition (CVD) processes using  $C_2H_2/H_2/Ar$  air flow were utilized based on adaptation from previous work.<sup>24</sup> The multilayered graphene was grown by heating a quartz tube furnace to 850 °C at atmospheric pressure with Ar and  $H_2$  flowing at 500 sccm and 100 sccm respectively, annealing for 5 minutes, pulling vacuum to 15 Torr and introducing  $C_2H_2$  at 2 sccm, while changing other gas flow rates to 250 sccm (Ar) and 50 sccm ( $H_2$ ). Following growth, the  $H_2$  and  $C_2H_2$  flows were halted and the furnace was cooled and sample removed. For the ultrathin graphite material growth, the process was generally the same, except the  $C_2H_2$  was introduced at 550 °C (7 sccm) at atmospheric pressure, and then the temperature was ramped to 750 °C. Additionally, the sample was supported by a ceramic sample boat to produce ultrathin graphite, which enabled slower cooling rates and much thicker graphitic precipitates. For ultrathin graphite foams, these materials were notably thick enough to maintain the exact replica of the original Ni foam template. In all cases, growth substrates were 110 ppi foams obtained from Winfay materials (China).

To form graphene-SWNT hybrid materials, we utilized electrophoretic deposition (EPD) of SWNTs<sup>25, 26</sup> dispersed in *n*-methylpyrrolidone (NMP) suspensions<sup>27</sup> to assemble a thin coating of SWNT bundles uniformly on the surface of the graphene foam. The SWNTs (HiPCO, purified, Unidym) were dispersed in NMP polar solvents with a 1 mg/mL SWNT concentration and sonicated for 30 minutes prior to EPD coating. The EPD coating process was performed with a stainless steel counterelectrode arranged 0.5 cm from the foam substrate, and deposition took place at 40 V using a DC power supply. This route involves no use of surfactants and after etching the Ni foam substrate in HCl, leaves a clean material free of surface contamination or oxygen species that can lead to adverse SEI formation and irreversible capacities. In cases where

we utilized (i) graphene or (ii) SWNT foams, we (i) performed the same multilayered graphene growth with no SWNT coating step, or (ii) utilized EPD to directly form coatings of clean NMP-suspended SWNTs on the Ni foam without the CVD graphene growth. After material assembly, we then dissolved away the Ni foam using a 1 M HCl bath for 48 hours, after which the samples were rinsed in a water bath and dried under vacuum.

### **Battery Fabrication and Electrochemical Testing**

Following the development of freestanding foam materials, coin cells were developed where these materials were utilized as a negative electrode in a half-cell configuration. This involved a standard 1 M LiPF<sub>6</sub> in ethylene carbonate/dimethyl carbonate electrolyte solution, a Celgard battery separator, and a lithium metal foil cathode. Electrochemical testing was performed using a Metrohm Autolab multichannel testing system, which included both cyclic voltammetry and Galvanostatic testing.

### **III. Results and Discussion**

The general process for making hybrid graphene-SWNT foams starting from Ni foams, CVD coating of graphene, and EPD coating of SWNTs is illustrated in Figure 1. After dissolving the Ni foam template, we find these materials to be freestanding and capable of flexure without damage (Fig. 1G). Scanning electron microscopy (SEM) images taken at low-magnification emphasize the structural characteristics of the foam materials that resemble the initial nickel foam from which they are derived (Figs. 1E-F). Shown in Figure 2A is a SEM image of a freestanding hybrid graphene-SWNT foam emphasizing the thin, conformal nature of the SWNT EPD coatings. Shown in Figs. 2B-C are representative high resolution transmission electron microscope (HR-TEM) images of edges in few-layered graphene sheets in graphene-SWNT hybrid materials emphasizing the low-defect and pristine graphene chemical structure.

Fast Fourier Transform (FFT) analysis of these HR-TEM images yielded an interlayer spacing of  $\sim 0.34$  nm for both the graphene-SWNT hybrid materials and the graphene foam materials without the presence of SWNTs, with FFTs and interlayer maps for both materials in supporting information. Previous work has emphasized a compromised interlayer spacing and defect formation when combining graphene with CNTs.<sup>16</sup> We do not observe such an effect, and attribute this to the pristine materials utilized in our study and the lack of aggressive processing methods, such as sonication, to prepare hybrid materials. We further performed Raman spectroscopic characterization with 785 nm excitations of both the pristine graphene and graphene-SWNT hybrid material. Evident from these spectra is a nearly indistinguishable D-band ( $1309\text{ cm}^{-1}$ ) in the graphene material and an  $I_{2D}/I_G$  ratio ( $2616\text{ cm}^{-1}$ ) indicative of few-layered graphene materials. Upon the deposition of SWNTs in the hybrid material, features arising from the resonant coupling of SWNTs with laser excitations include a slight increase in the D band, the emergence of low-frequency radial breathing modes, and a depression of the  $I_{2D}/I_G$  ratio ( $2578\text{ cm}^{-1}$ ). The comparative Raman spectra from SWNTs and ultra-thin graphite are included in the supporting information.

To assess the electrochemical performance of these materials as anodes for Li-ion batteries, freestanding carbon nanomaterial foam half-cells were then subjected to Galvanostatic charge-discharge testing at charging currents ranging from 0.186 A/g to 27.9 A/g (0.5C and 75C respectively for a standard graphite anode) from 0 – 3.7 V (vs. Li/Li<sup>+</sup>). Shown in Figure 3A are rate capability curves for Li storage in freestanding anode materials composed of graphene, graphene-SWNT hybrids, SWNT, and ultrathin graphite. The ultrathin graphite material, which is composed of 50-200 nanometers of graphite material in the same 3-D foam geometry, exhibits performance characteristic of bulk 3-D graphite materials with a maximum observed capacity of

332 mAh/g at a rate of C/4 and 260 mAh/g at a rate of C/2, consistent with the performance of a bulk carbon anode in a Li-ion battery. Multilayered graphene and SWNT materials exhibit capacities of 1076 and 1299 mAh/g at the same C/2 rate (0.186 A/g), and when combining these materials into hybrid structures we observe reversible capacities of up to 2640 mAh/g at 0.186 A/g (over 1:1, Li:C), which remains 236 mAh/g at 27.9 A/g, respectively. To our knowledge, this is both the highest rate capability and capacity measured for carbon nanomaterials, and the freestanding, 3-D, conductive, and flexible nature of these materials enables the possibility for their direct integration into packaged cells without additional metallization or use of binders.

As many high capacity anode materials are subject to rapid performance degradation, we find these materials (hybrid graphene-CNT) to exhibit excellent cycling performance measured over 300 charge-discharge cycles by performing 100 cycles on a single device at three different rates (Fig. 3b). We observed no capacity fade over cycling studies, (0.74 A/g, 7.4 A/g, and 14.8 A/g), and even observe the capacity to slightly increase upon cycling, especially at slow charging rates. This has been previously observed in CVD graphene materials and attributed to continuous activation of graphene storage activity during cycling.<sup>10</sup> Our studies indicate ~ 2X higher discharge capacity between the first and second cycles as indicated in other studies (supporting information), but cycling appears to improve this storage capacity to a value intermediate of these. Whereas a mechanistic understanding of this effect remains elusive, we speculate the improvement upon cycling to represent an evolution of the SEI layer on sp<sup>2</sup> hybridized carbon surfaces to compliment improved storage in contrast to the inhibitory effect the SEI plays in other storage media. In this manner, this is particularly attributed to the sp<sup>2</sup> nature of the carbon in our devices and a characteristic of surface-based metal storage that is yet to be completely understood. Another possibility we speculate could be cycling induced wetting

of electrolyte into the torturous graphene-CNT material, as the high surface free-energy of an  $sp^2$  hybridized carbon material inhibits spontaneous wetting. Whereas this effect is most pronounced at the slowest cycling rates, it occurs at all rates studied and was not found to saturate in the course of our cycling experiments. Notably, the best measured reversible capacities in Fig. 3A were obtained after device cycling, representing the potential for even better performance from these hybrid materials.

To understand the electrochemical performance of hybrid graphene-SWNT materials as Li-ion battery anodes, Galvanostatic charge-discharge curves (Figure 4) and corresponding cyclic voltammetry (CV) curves (Figure 5) were analyzed for all materials studied. For discharge curves at 0.186 A/g (labeled 0.19 A/g), we observe a low-voltage ( $< 0.5$  V) plateau for the three samples containing graphene or graphite (Fig. 4) with a corresponding low-voltage peak in the CV scans taken at 0.5 mV/second rates (Fig. 5). This can be attributed to intercalation of lithium into the subsurface layers of the multilayered graphene or graphite in a manner reflecting  $LiC_6$  bulk storage. At 0.186 A/g, the low-voltage plateau accounts for  $\sim 150$  mAh/g charging capacity for ultra-thin graphite, and between 150-250 mAh/g capacity for the graphene and graphene-SWNT hybrid materials – slightly greater due to the rapidly accessible bulk layers in the multilayered graphene. In comparison, the SWNT foam exhibited no observable signature of chemical storage in this low-voltage regime. This confirms that (i) the enhanced performance in hybrid materials is not related to bulk intercalation of Li species, and (ii) pure SWNT materials exhibit no conventional bulk-like intercalation.

Electrochemical measurements at voltages from 1 – 3.7 V (vs.  $Li/Li^+$ ) give key insight into differentiating features in storage capacity between the different materials. Li-storage in nanostructured carbons in this window has been previously associated with Faradaic charge

transfer reactions between the electrolyte species and the edges or surface sites of the graphene or SWNT materials. Density functional theory calculations have emphasized the mediation of these Faradaic reactions through defect or  $sp^3$  carbon sites.<sup>28</sup> Whereas ultra-thin graphite shows little storage in this regime (Fig. 4B, 5B), the SWNT, graphene, and graphene-SWNT hybrid foam materials are specifically distinguished in this regime by their storage capability with the graphene-SWNT hybrid exhibiting superior Faradaic charge storage performance. For the SWNT foams, a plateau (Fig. 4C) and bump (Fig. 5C) from 1-2.2 V (vs. Li/Li<sup>+</sup>) during charging represents the primary Faradaic charge storage reaction. This is compared to graphene foams that exhibit a small plateau between 1-2.2 V (Fig. 4A), with more contribution from Li storage at higher voltages. For the hybrid graphene-SWNT material, both a greater plateau from 1-2.2 V is observed compared to the SWNT foams, and more storage above 2.2 V is also observed (Figs. 4D, 5D). From this result, we infer that the SWNT materials enable a lower-energy chemical pathway for LiPF<sub>6</sub> decomposition and corresponding Faradaic Li storage than graphene, with charge capacity of the SWNTs dictated by the area under the peak in the positive CV scan in Fig. 5 (illustrated in Fig. 6A). In contrast, the graphene materials exhibit a less well-defined energy regime for Li storage and significantly more Faradaic charge-transfer reactions at voltages above 2 V. Therefore, the electrochemical characteristics of SWNTs and graphene are complimentary for Li storage, as SWNTs enable reactivity with the electrolyte to chemisorb Li species, and graphene materials provide a surface topology capable of reaching high storage capacities (Fig. 6). Once the Li species are formed on the SWNT surface, they can rapidly diffuse to occupy sites on the graphene material.<sup>23</sup> Previous studies focused on chemical functionalization of graphene surfaces have noted the extreme low reactivity of  $sp^2$ , flat, basal plane graphene in comparison to defect sites, edges, and ripples in the graphene material.<sup>29-31</sup> Compared to flat

graphene, SWNTs exhibit greater reactivity in charge-transfer reactions due to their curvature-induced higher surface free energy.<sup>32</sup> Based on this, we propose here that the mechanism for the enhanced storage in graphene-SWNT hybrid materials is the capability to use a hybrid system to decouple electrolyte decomposition reaction energetics and surface storage capacity in an anode material without compromising the low-defect  $sp^2$  characteristics of the surface carbons. This is consistent with previous studies arguing the importance of defects for Li storage on graphene<sup>10, 20</sup> since defect and edge sites in graphene can play a similar role as SWNTs (illustrated in Fig. 6A) to facilitate Faradaic charge-transfer reactions. However, defects and edges in a graphene anode are likely to require the forfeit of some irreversible capacity due to the strong binding between chemical species and  $sp^3$  carbons that isn't present when utilizing low-defect  $sp^2$  carbon hybrid material. As a result, hybrid materials enable one to decouple the function of the individual materials in an anode to engineer optimized storage without compromising the total reversible storage capacity of the graphene material – the mechanism we propose to yield excellent storage characteristics in our hybrid material.

Finally, the graphene-SWNT material also exhibits extraordinary rate capability at high currents. At a cycling rate of 27.9 A/g, specific capacities are measured of 236 mAh/g. CV scans at fast scan rates isolate this as surface Faradaic reactions (Fig. S4), and half-cell power densities greater than 30 kW/kg are measured (Fig. S6) indicating power capability comparable to the best supercapacitors. To emphasize the rate capability of this device, if a graphene supercapacitor was achieved with a specific capacitance of 550 F/g (the highest achievable value) at 27.9 A/g, its capacity at 1 V would be almost 1.5X smaller than the hybrid graphene-SWNT device. Furthermore, a commercial cell utilizing this battery anode, if rated for a maximum capacity of 2640 mAh/g, could reach full charge at 27.9 A/g in just over 5 minutes –

perhaps similar to the length of time it takes to currently fill a fuel tank in a gas-powered automobile. This is achieved by the nanoengineering of complimentary functions of carbon nanostructures in hybrid materials into ultrahigh performance electrodes – a concept that we anticipate to be broadly transferrable to other systems such as Li-air batteries, chemical and biological sensors, electrochemical solar cells, and catalysis.

#### **IV. Conclusions**

We demonstrate the ability to utilize a hybrid graphene-SWNT freestanding material to enable high capacity lithium storage approaching the most ideal bulk storage materials, but with a tunable electrode-electrolyte surface reactivity based on the SWNTs in the hybrid material. This enables us to achieve ultrahigh storage capacities in hybrid structures (2640 mAh/g, 0.186 A/g), but also to maintain excellent rate performance (236 mAh/g, 27.6 A/g). Such a route to develop hybrid assemblies of nanostructures that can decouple the surface electrode-electrolyte reactivity from the total electrode storage capacity gives credence to the realization of carbon nanostructured materials as practical energy carriers for use in lithium-ion batteries. As we demonstrate in this work, such materials give promise to a simultaneous 10X greater capacity and over 10X faster charging rate than that which can be achieved with conventional battery technology.

#### **Acknowledgements**

The authors would like to thank Avetik Harutyuntan (Honda Research Institute), Dave Geohegan, and Alex Puzetky (ORNL) for useful discussions. TEM images obtained in this study were made possible by an instrument funded by NSF grant EPS 1004083. L.O. was supported by NSF grant CMMI 1334269, and this work was supported in part by Vanderbilt

start-up funds and an Oak Ridge Associated Universities Powe Award. SEM characterization parts of this work were conducted at the Center for Nanophase Materials Sciences, which is sponsored at Oak Ridge National Laboratory by the Scientific User Facilities Division, Office of Basic Energy Sciences, U.S. Department of Energy.

**Supporting Information** is available that includes (i) SEM and photographs of ultra-thin graphite foams, (ii) Raman spectra from SWNT and ultrathin graphite foams, (iii) CV measurements at higher scan rates, (iv) Comparison of discharge characteristics of first, second, and 300<sup>th</sup> discharge, (v) Ragone plot showing power-energy characteristics of hybrid graphene-SWNT electrodes, and (vi) TEM images of multilayered graphene edges from graphene and graphene-SWNT hybrids, with interlayer spacing maps and FFT analysis.

## Figures

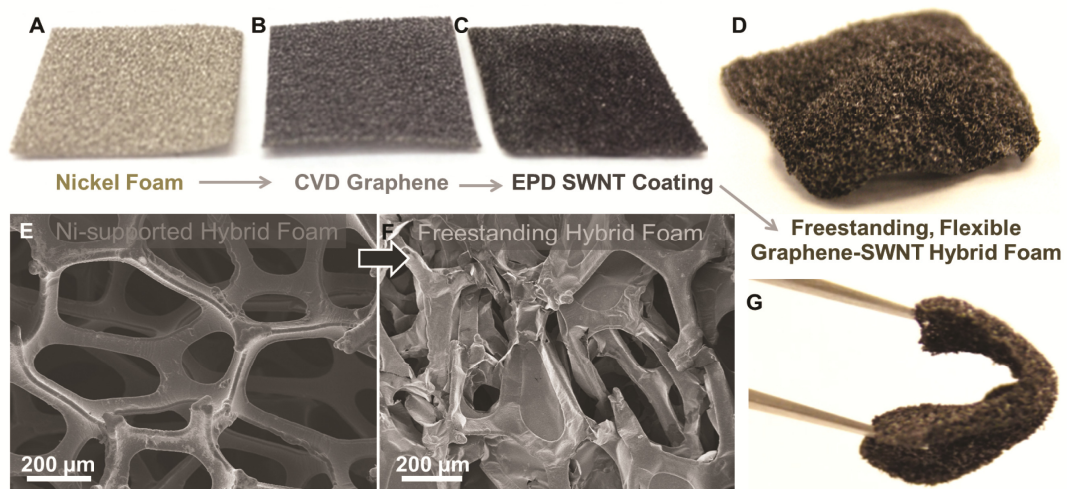


Figure 1

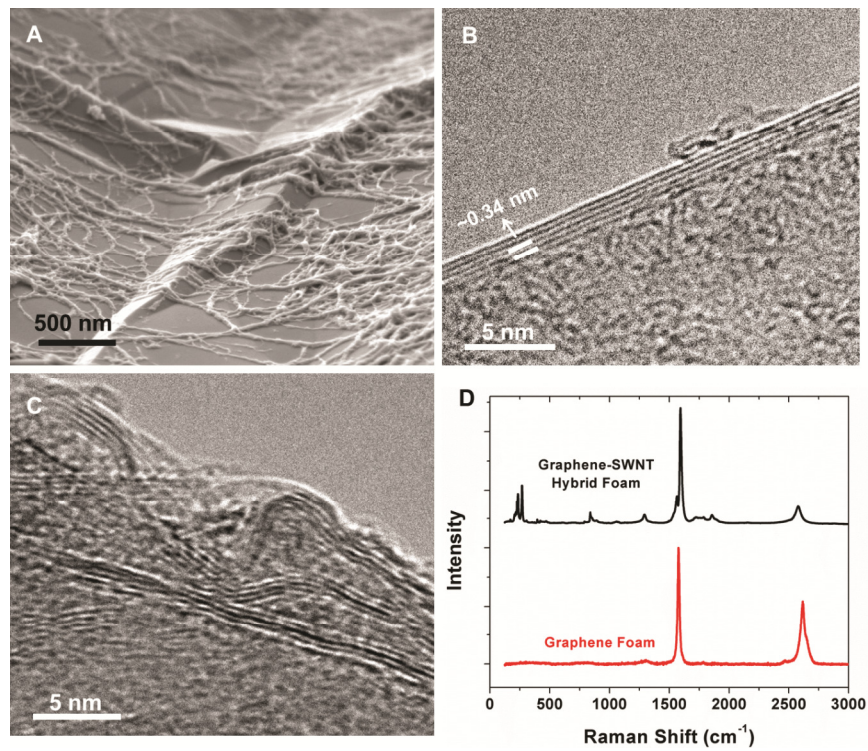


Figure 2

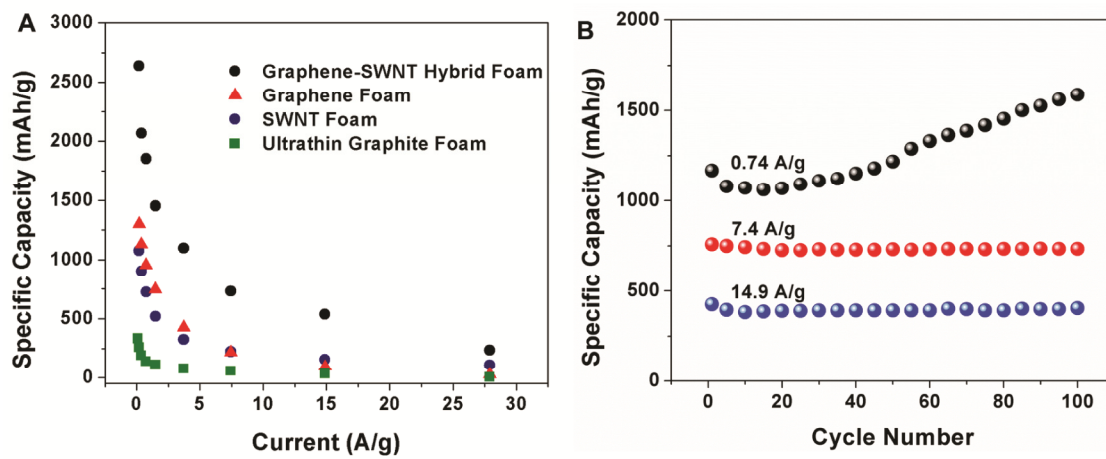


Figure 3

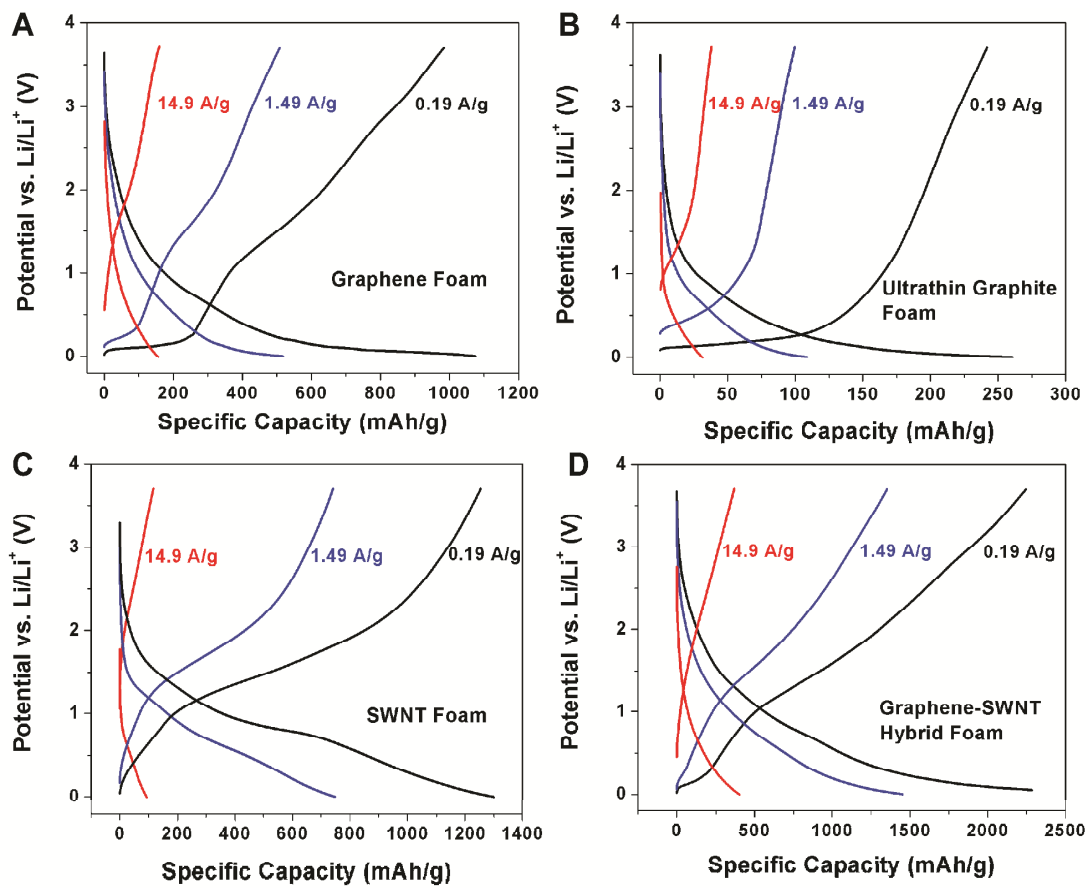


Figure 4

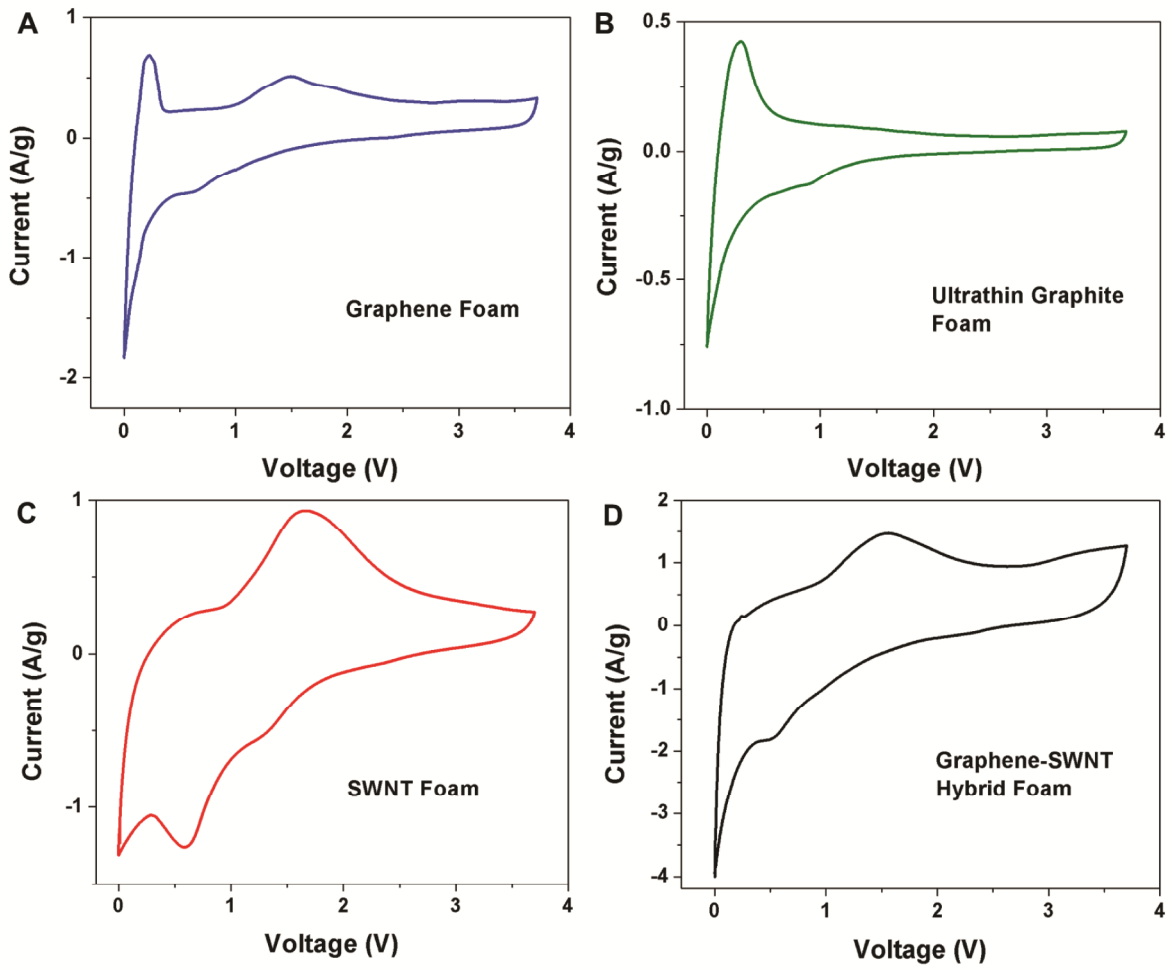


Figure 5

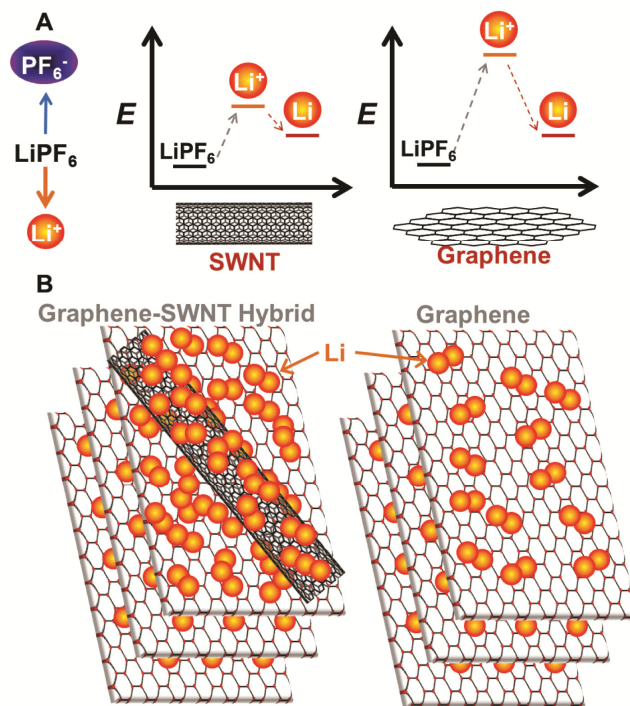


Figure 6

## Figure Captions

**Figure 1.** (A-D) Pictures of the materials formed during steps associated with the fabrication of 3-D freestanding hybrid graphene-SWNT foams starting from (A) nickel foam, (B) nickel foam after CVD coating of graphene, (C) the graphene/nickel foam material after EPD of a thin layer of SWNTs, and (D) the freestanding graphene-SWNT foam after dissolution of Ni in HCl. (E-F) SEM images of (E) nickel-foam supported graphene-SWNT hybrid materials, and (F) freestanding graphene-SWNT hybrid materials. (G) Photograph showing the flexure of a foam material at over a  $90^\circ$  angle, emphasizing the mechanical rigidity and flexibility of the material.

**Figure 2.** (A) SEM images of hybrid graphene-SWNT materials emphasizing the thin, pristine coating of SWNTs, (B-C) TEM images isolating graphene materials in graphene-SWNT hybrid structures. Interlayer spacing of  $\sim 0.34$  nm was determined using FFT analysis (supporting information), and (D) Raman spectroscopic characterization (532 nm) of 3-D graphene and graphene-SWNT hybrid foam materials.

**Figure 3.** (A) Rate capability plot showing the specific capacity (mAh/g) as a function of the Galvanostatic charge-discharge current in A/g for the four freestanding foam materials studied in this work. (B) Cycle lifetime study of graphene-SWNT hybrid materials cycled at rates of 0.74, 7.4, and 14.9 A/g (corresponding to 2C, 10C, and 20C for graphite materials).

**Figure 4.** Galvanostatic charge-discharge measurements at cycling rates of 14.9, 1.49, and 0.19 A/g for (A) graphene foams (B) ultrathin graphite foams, (C) pristine SWNT foams, and (D) hybrid graphene-SWNT foams.

**Figure 5.** Cyclic voltammetry curves at scan rates of 0.5 mV/second for (A) graphene foams, (B) ultrathin graphite foams, (C) pristine SWNT foams, and (D) hybrid graphene-SWNT foams. CV curves at higher scan rates are included in the supporting information.

**Figure 6.** (A) Proposed conceptual energy diagrams of the chemical pathways for Li storage on defect-free SWNT and graphene surfaces emphasizing the improved reactivity of SWNTs, and (B) schematic illustrated the improve capacity of graphene-SWNT hybrids based on the process illustrated in (A).

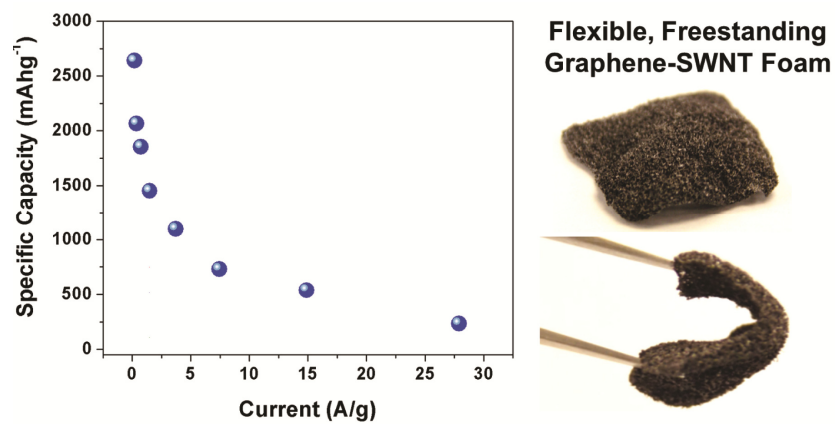
## References

1. A. S. Arico, P. Bruce, B. Scrosati, J. M. Tarascon and W. Van Schalkwijk, *Nat Mater*, 2005, **4**, 366-377.
2. M. Armand and J. M. Tarascon, *Nature*, 2008, **451**, 652-657.
3. P. G. Bruce, B. Scrosati and J. M. Tarascon, *Angew Chem Int Edit*, 2008, **47**, 2930-2946.
4. J. M. Tarascon and M. Armand, *Nature*, 2001, **414**, 359-367.
5. C. K. Chan, H. L. Peng, G. Liu, K. McIlwrath, X. F. Zhang, R. A. Huggins and Y. Cui, *Nat. Nanotechnol.*, 2008, **3**, 31-35.
6. R. Teki, M. K. Datta, R. Krishnan, T. C. Parker, T. M. Lu, P. N. Kumta and N. Koratkar, *Small*, 2009, **5**, 2236-2242.
7. N. A. Kaskhedikar and J. Maier, *Adv. Mater.*, 2009, **21**, 2664-2680.
8. C. Liu, F. Li, L. P. Ma and H. M. Cheng, *Adv. Mater.*, 2010, **22**, E28.
9. S. Chen, P. Bao, L. Xiao and G. Wang, *Carbon*, 2013, **64**, 158-169.
10. Z. J. Fan, J. Yan, G. Q. Ning, T. Wei, L. J. Zhi and F. Wei, *Carbon*, 2013, **60**, 558-561.
11. Y. Gong, S. Yang, Z. Liu, L. Ma, R. Vajtai and P. M. Ajayan, *Adv. Mater.*, 2013, **25**, 3979-3984.
12. Y. Hu, X. Li, J. Wang, R. Li and X. Sun, *J. Power Sources*, 2013, **237**, 41-46.
13. H. X. Ji, L. L. Zhang, M. T. Pettes, H. F. Li, S. S. Chen, L. Shi, R. Piner and R. S. Ruoff, *Nano Lett*, 2012, **12**, 2446-2451.
14. D. Y. Pan, S. Wang, B. Zhao, M. H. Wu, H. J. Zhang, Y. Wang and Z. Jiao, *Chem Mater*, 2009, **21**, 3136-3142.
15. Z.-S. Wu, W. Ren, L. Xu, F. Li and H.-M. Cheng, *ACS Nano*, 2011, **5**, 5463-5471.

16. E. Yoo, J. Kim, E. Hosono, H. Zhou, T. Kudo and I. Honma, *Nano Lett*, 2008, **8**, 2277-2282.
17. G. X. Wang, X. P. Shen, J. Yao and J. Park, *Carbon*, 2009, **47**, 2049-2053.
18. P. Guo, H. H. Song and X. H. Chen, *Electrochem. Commun.*, 2009, **11**, 1320-1324.
19. P. C. Lian, X. F. Zhu, S. Z. Liang, Z. Li, W. S. Yang and H. H. Wang, *Electrochim. Acta*, 2010, **55**, 3909-3914.
20. X. F. Li, Y. H. Hu, J. Liu, A. Lushington, R. Y. Li and X. L. Sun, *Nanoscale*, 2013, **5**, 12607-12615.
21. X. F. Fan, W. T. Zheng, J. L. Kuo and D. J. Singh, *ACS Appl. Mater. Inter.*, 2013, **5**, 7793-7797.
22. A. M. Garay-Tapia, A. H. Romero and V. Barone, *J. Chem. Theory Comput.*, 2012, **8**, 1064-1071.
23. C. Uthaisar and V. Barone, *Nano Lett*, 2010, **10**, 2838-2842.
24. Z. P. Chen, W. C. Ren, L. B. Gao, B. L. Liu, S. F. Pei and H. M. Cheng, *Nat Mater*, 2011, **10**, 424-428.
25. A. R. Boccaccini, J. Cho, J. A. Roether, B. J. C. Thomas, E. J. Minay and M. S. P. Shaffer, *Carbon*, 2006, **44**, 3149-3160.
26. L. Oakes, A. Westover, M. Mahjouri-Samani, A. A. Puretzky, C. Rouleau, D. B. Geohegan and C. L. Pint, *ACS Appl. Mater. Inter.*, 2013, **5**, 13153-13160.
27. Y. Hernandez, V. Nicolosi, M. Lotya, F. M. Blighe, Z. Y. Sun, S. De, I. T. McGovern, B. Holland, M. Byrne, Y. K. Gun'ko, J. J. Boland, P. Niraj, G. Duesberg, S. Krishnamurthy, R. Goodhue, J. Hutchison, V. Scardaci, A. C. Ferrari and J. N. Coleman, *Nat. Nanotechnol.*, 2008, **3**, 563-568.

28. L. J. Zhou, Z. F. Hou and L. M. Wu, *J. Phys. Chem. C*, 2012, **116**, 21780-21787.
29. Z. Z. Sun, C. L. Pint, D. C. Marcano, C. G. Zhang, J. Yao, G. D. Ruan, Z. Yan, Y. Zhu, R. H. Hauge and J. M. Tour, *Nat. Commun.*, 2011, **2**.
30. Z. Z. Sun, D. K. James and J. M. Tour, *J. Phys. Chem. Lett.*, 2011, **2**, 2425-2432.
31. K. P. Loh, Q. L. Bao, P. K. Ang and J. X. Yang, *J. Mater. Chem.*, 2010, **20**, 2277-2289.
32. S. Park, D. Srivastava and K. Cho, *Nano Lett*, 2003, **3**, 1273-1277.

## Color Table of Contents Graphic



Text: Freestanding, flexible graphene-SWNT foams give promise for Li-ion batteries due to synergistic roles of these hybrid materials in Li storage.